PHYSICAL REVIEW A **91**, 061402(R) (2015)

Fast production of Bose-Einstein condensates of metastable helium

Q. Bouton, R. Chang, A. L. Hoendervanger, F. Nogrette, A. Aspect, C. I. Westbrook, and D. Clément
Laboratoire Charles Fabry, Institut d'Optique, CNRS, Université Paris Sud, 2 Avenue Augustin Fresnel, F-91127 Palaiseau Cedex, France
(Received 30 April 2015; published 9 June 2015)

We report on the Bose-Einstein condensation of metastable ^{4}He atoms using a hybrid approach, consisting of a magnetic quadrupole and an optical dipole trap. In our setup we cross the phase transition with 2×10^6 atoms, and we obtain pure condensates of 5×10^5 atoms in the optical trap. This approach to cooling ^{4}He provides enhanced cycle stability, large optical access to the atoms and results in the production of a condensate every 6 s—a factor 2 faster than the state of the art. This speed-up will significantly reduce the data acquisition time needed for the measurement of many particle correlations, made possible by the ability of metastable helium atoms to be detected individually.

DOI: 10.1103/PhysRevA.91.061402 PACS number(s): 37.10.De, 37.10.Gh, 05.30.Jp

In the study of many physical phenomena, one often seeks to make highly accurate measurements or search for rare events. In these situations convincing evidence can only be obtained by acquiring a large amount of data to increase the statistical significance of the results. Multiparticle correlations are a good example of such measurements and are often used in both particle physics [1] and quantum optics [2,3]. Thus efforts to increase data acquisition rates often constitute a major preoccupation for experimentalists.

In the field of ultracold gases recent advances in imaging techniques have permitted the detection of individual atoms and the measurement of their correlations [4–11]. Because of the electronic detection techniques enabled by the use of metastable helium He*, significant contributions to this field have been made using this species [12–15]. However, these experiments are often limited by the stability of the apparatus over long data runs.

For many atomic species, the stability and cycle time have been dramatically improved by all-optical cooling [16,17] or by magnetic-optical hybrid traps [18]. Such techniques have yet to be realized in He*, in part because of significant challenges posed by the unusual characteristics of this atom. In unpolarized He*, the density is severely limited by Penning collisions [19–22] preventing the use of all-optical cooling techniques without spin polarization. Hybrid traps use magnetic quadrupoles in which one must minimize losses due to Majorana spin flips. Since the Majorana loss rate, at a given temperature, varies inversely with the particle mass [23], He* is particularly unfavorable for this approach as well. Nevertheless the potential gain offered by these novel approaches is sufficiently great that it is worth some effort to try to circumvent these difficulties.

Here we report the implementation of a hybrid approach to Bose-Einstein condensation (BEC) of helium in the metastable state (^{4}He*), permitting fast and robust production of condensates with 5×10^5 atoms every 6 s. We demonstrate that the use of a quadrupole magnetic trap (QMT) in place of the Ioffe or cloverleaf configurations used in other ^{4}He* experiments [24–30] offers technical simplicity, enhanced stability, and shorter cycle time—a factor 2 speed-up over the state of the art. Starting from a magneto-optical trap, our experimental cycle consists of laser cooling in optical molasses (Doppler and gray molasses), compression, and radio-frequency evaporation in a QMT, transfer into a crossed optical dipole trap (ODT) by opening the QMT, and final forced evaporation to BEC. The cloud properties throughout the cooling cycle are summarized in Table I, and the atom number N and phase-space density $\mathcal{D}$ are plotted in Fig. 1. As it can be seen from Table I, each step of the cycle gives a substantial contribution towards the fast production of BECs.

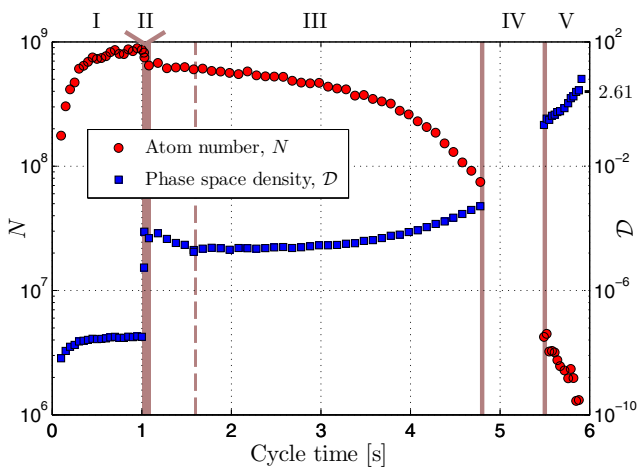

FIG. 1. (Color online) Atom number N (red circles) and phase space density $\mathcal{D}$ (blue squares) through the experimental cycle. The scheme is divided in stages: (I) Magneto-optical trap loading and compression, (II) Doppler and gray molasses cooling, (III) compression and radio-frequency evaporation in a quadrupole magnetic trap (QMT), (IV) transfer from the QMT to the optical dipole trap (ODT) by adiabatically lowering the QMT field, and (V) forced evaporation in the crossed ODT to Bose-Einstein condensation.

Magneto-optical trapping and laser cooling. The first stage has been described in detail in [31]. Briefly, a six-beam MOT of ^{4}He* atoms is loaded from a dc-discharge plasma source, followed by transverse (molasses) and longitudinal (Zeeman slower) cooling. The MOT is composed of a quadrupole magnetic field with gradient $B' = 25$ G/cm (strong axis) and light red-detuned by $\Delta = -31\Gamma$ ($\Gamma/2\pi = 1.6$ MHz) from the $2\,^3S_1 \rightarrow 2\,^3P_2$ resonance and at a high intensity of 50 I_{sat} per beam ($I_{\mathrm{sat}} = 0.16$ mW/cm^2). This configuration provides a large capture velocity while keeping the cloud density low so to reduce losses due to light-assisted Penning collisions [19–21]. MOTs with $N \sim 9 \times 10^8$ atoms at a temperature of $T = 1.2$ mK are loaded in 1 s [32]. The MOT is then compressed

TABLE I. Measured cloud parameters following each phase of the cooling cycle. We present the atom number N, temperature T, peak density ρ_0, and phase space density $\mathcal{D}$.

Experimental steps	N	T (μK)	ρ_0 (cm^{-3})	$\mathcal{D}$
Magneto-optical trap	$8.7(2) \times 10^8$	1200(100)	$2.5(1) \times 10^9$	$4.0(4) \times 10^{-8}$
Red molasses	$8.2(1) \times 10^8$	120(11)	$1.1(1) \times 10^{10}$	$5.5(6) \times 10^{-6}$
Gray molasses	$7.5(2) \times 10^8$	20(3)	$1.1(1) \times 10^{10}$	$7.8(7) \times 10^{-5}$
Quadrupole trap loading	$6.4(2) \times 10^8$	38(3)	$2.0(2) \times 10^{10}$	$5.5(2) \times 10^{-5}$
Quadrupole trap compression	$6.1(1) \times 10^8$	230(15)	$1.0(1) \times 10^{11}$	$2.0(3) \times 10^{-5}$
Radio-frequency evaporation	$6.0(1) \times 10^7$	70(6)	$3.3(6) \times 10^{11}$	$3.7(7) \times 10^{-4}$
Optical dipole trap loading	$5.0(2) \times 10^6$	27(2)	$5.1(2) \times 10^{13}$	$2.4(3) \times 10^{-1}$

by ramping the detuning Δ from -31Γ to -2Γ in 20 ms. At the same time, the light intensity is reduced from 50 $I_{\rm sat}$ to 0.33 $I_{\rm sat}$ to keep the rate of light-induced Penning collisions low. At the end of this phase, we have increased the density by a factor $\simeq$9 while losing a small fraction of atoms (10%).

After the compression we further cool the cloud in an optical molasses. We use a red molasses to capture the atoms from the MOT and then load them into a gray molasses to reach low temperatures. Although it is possible to cool ^{4}He* on the $2\,^3S_1 \rightarrow 2\,^3P_2$ transition to the Doppler limit ($T_D = \hbar\Gamma/2k_B = 38$ μK) [31], we cool only to 120 μK in 5 ms, a value that is sufficiently low to load a blue-detuned gray molasses on the $2\,^3S_1 \rightarrow 2\,^3P_1$ transition. Three-dimensional cooling of helium gases with blue-detuned molasses has been demonstrated in the past [33]. While sub-Recoil cooling was achieved, only a small fraction of 10^4 atoms were brought to these ultralow temperatures. Here the parameters we choose (laser detuning $\Delta' = +10\Gamma$ and intensity of 20 $I_{\rm sat}$) allow us to capture nearly all the atoms from the red molasses and cool $N = 7.5 \times 10^8$ atoms to a temperature of $T = 20$ μK in 5 ms. At this stage the low atomic density $\rho_0 \simeq 1.1 \times 10^{10}$ cm^{-3}, limited by light-induced Penning collisions in the MOT, prevents us from efficiently loading an optical dipole trap. On the other hand, a spin-polarized helium gas in the absence of near-resonant light has a significantly smaller inelastic collision rate [34]. Thus we load the atoms into a magnetic trap where the atomic density can be increased in order to facilitate efficient transfer into the optical trap.

QMT loading and compression. We first optically pump a large fraction of the atoms ($\sim$85%) to the $J = 1$ $m_J = 1$ state. The gas is then captured by abruptly turning on a magnetic field gradient of $B' = 4.5$ G/cm. The magnetic field is produced by the pair of coils in anti-Helmholtz configuration used for the MOT. Next we adiabatically ramp up the field to $B' = 45$ G/cm over 500 ms in order to increase the density and thus the elastic collision rate. At this point there are $N = 6 \times 10^8$ atoms in the compressed cloud at a temperature of $T = 230$ μK, corresponding to a phase space density of $\mathcal{D} = 2.0 \times 10^{-5}$.

A well-known issue with the QMT is the existence of a magnetic field zero at the center of the trap, which can lead to Majorana spin flips to an un-trapped magnetic sub-state [23]. At a given temperature the rate of spin flips scales inversely with the particle mass and thus is particularly strong for helium. The effects of Majorana spin flips are twofold: First they result in loss of atoms, as atoms escape from the $m_J = 1$ trapped state to the un-trapped states ($m_J = 0$ and $m_J = -1$). The Majorana loss rate is [35,36]

$$\Gamma_m = \chi \frac{\hbar}{m} \left(\frac{\mu B'}{k_B T} \right)^2, \tag{1}$$

where k_B is the Boltzmann constant, B' the magnetic gradient along the coil axis, $\mu = 2\mu_B$ the magnetic moment, μ_B the Bohr magneton, $\hbar$ Planck's constant, m the particle mass, and χ a dimensionless geometrical factor. Secondly, this loss results in a heating of the cloud, as it is typically the coldest atoms, that stay around the field zero, that are lost. This change in temperature results in a nonexponential decay of the atom number N (see the inset of Fig. 2). The temperature evolution is expected to follow a simple law [37]:

$$T(t) = \sqrt{T_0^2 + \gamma_m t}, \tag{2}$$

with

$$\gamma_m = \frac{8}{9} \chi \frac{\hbar}{m} \left(\frac{\mu B'}{k_B} \right)^2, \tag{3}$$

where T_0 is the initial temperature at $t = 0$.

We monitor the cloud temperature as a function of time in a fixed magnetic trap and for different initial temperatures T_0. Our measurements, shown on Fig. 2, are in excellent agreement

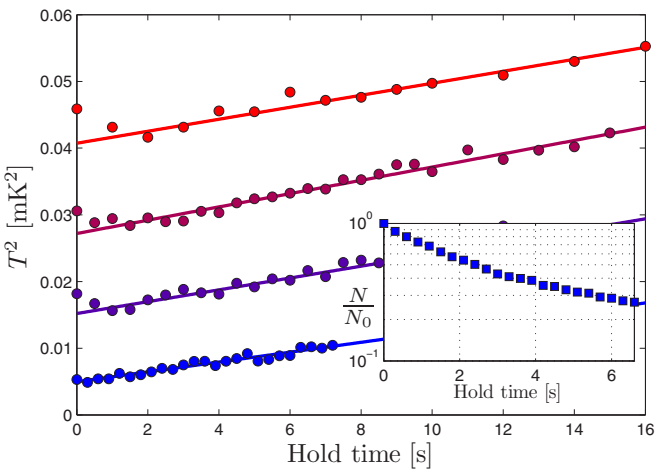

FIG. 2. (Color online) Time evolution of the square of the cloud temperature T in a QMT with fixed $B' = 45$ G/cm and for varying initial temperatures $T_0 = 202, 165, 123$, and 70 μK (dots). Lines are fits according to Eq. (2) from which we extract a geometrical factor $\chi = 0.17(2)$. (Inset) Evolution of the atom number in the QMT for the data set with $T_0 = 70$ μK.

with the prediction of Eq. (2), with a fitted geometrical factor $\chi = 0.17(2)$. This value agrees well with that reported for other species [35,37]. The measurement of the heating and atom loss rates allows us to tailor our compression and cooling cycle to minimize these negative effects. To this end, we compress the magnetic trap to a final gradient of only 45 G/cm. Even at this relatively weak gradient the density is increased by a factor 30 (see Table I) and the initial elastic collision rate of 170 s^{-1} (the vacuum lifetime is 50 s) is high enough to perform forced evaporation [38].

Radio-frequency evaporation in the QMT. Cooling in the QMT is performed by forced radio-frequency (RF) evaporation. The RF signal is generated by a National Instruments PXI-5406A arbitrary function generator and amplified to 50 W by a Prana DP140 RF amplifier. The field is generated by an RF coil outside the vacuum chamber, positioned 6 cm from the atoms. An RF field of frequency ν imposes a trap depth which is characterized by the cutting parameter $\eta = h\nu/k_B T$ [39]. Our ramp begins with a constant frequency of 34 MHz for 1 s followed by a linear sweep of the frequency from 34 to 8 MHz during 2.25 s. The RF cooling is summarized in stage III of Fig. 1 where the vertical dashed line marks the beginning of the RF evaporation. During this stage, the peak collision rate increases from 170 s^{-1} to 360 s^{-1}, while the Majorana loss rate Γ_m increases from 8.6×10^{-3} s^{-1} to 1.0×10^{-1} s^{-1}. The final cloud has $N = 6 \times 10^7$ atoms at a temperature of $T = 70\ \mu$K, with a peak atomic density $\rho_0 = 3.3 \times 10^{11}$ cm^{-3} below the densities at which inelastic two-body and three-body loss become important [25,27,28,40]. Having gained more than one order of magnitude in the density ρ_0, we begin the transfer into the optical trap.

Transfer to the optical dipole trap and Bose-Einstein condensation. The optical dipole trap is made of two Gaussian-shaped beams at 1550 nm (fiber laser source IPG ELR-30-1550-LP). The first beam has a power of 18 W, focused down to a waist of 133 μm. The second beam contains 8 W focused to a waist of 63 μm, and crosses the first beam at an angle of 40° in the horizontal plane. The resulting trap is roughly cylindrical with trap frequencies of 3.1 kHz radially and 624 Hz axially, and a trap depth of $U_0 = k_B \times 244\ \mu$K. The trap center is displaced roughly one beam waist below the quadrupole center to avoid accumulating atoms at the magnetic field zero.

The transfer from the QMT to the ODT is performed by ramping down the field gradient to 3 G/cm over 600 ms in the presence of the ODT (stage IV in Fig. 1), before abruptly switching it off. A small bias field maintains the spin polarization of the atoms in the ODT. Due to the overlap of magnetically trapped and optically trapped atoms during the transfer, images of the atom clouds are difficult to interpret quantitatively, hence it is only the start and end points which are shown in Fig. 1. We estimate there are up to 1.5×10^7 atoms at a peak density of $\rho_0 \simeq 10^{14}$ atoms/cm^3 initially in the crossed ODT. The atom number proceeds to decay rapidly due to a mixture of evaporative cooling and three-body loss [25,27,28]. After 20 ms the atom cloud equilibrates with $N = 5 \times 10^6$ atoms at a temperature of $T = 25\ \mu$K and a phase space density of $\mathcal{D} = 0.2$. Despite retaining only 10% of the atoms from the QMT, we observe a gain in phase space density of 3 orders of magnitude, similar to that reported in other hybrid trap setups [18]. This increase comes from a combination of a dimple effect (resulting in a dramatic increase in the atomic density) and subsequent evaporation in the crossed ODT. Interestingly the final atom number loaded in the ODT does not strongly depend on the efficiency of the previous RF evaporation. Indeed the ODT atom number is similar for the 3.25-s RF ramp (overall efficiency of $\gamma = -d \log \mathcal{D}/d \log N = 1.39$) as for a longer and more efficient 6.5-s ramp ($\gamma = 1.62$).

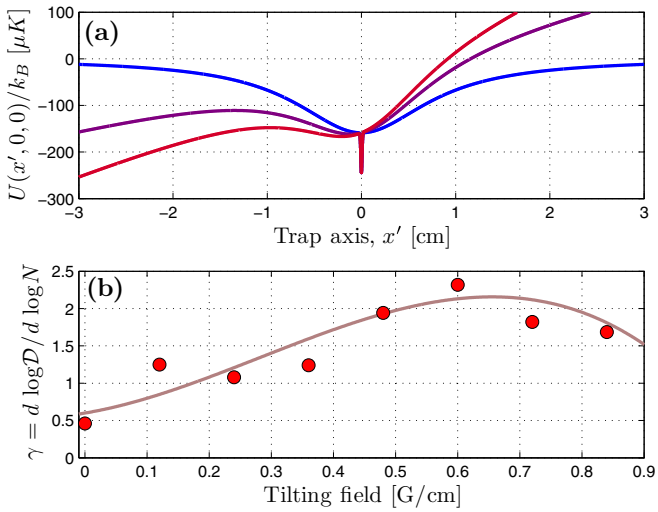

FIG. 3. (Color online) (a) ODT potential along the second beam axis and for tilting fields $B'_{\rm tilt} = 0$,0.4, and 0.6 G/cm (blue, purple, red). (b) ODT evaporation efficiency γ as a function of tilting field $B'_{\rm tilt}$. The solid line is a guide for the eye.

The final cooling stage is performed by ramping down the ODT powers over 500 ms from 18 and 8 W to 1 and 0.3 W, in beams 1 and 2, respectively. This evaporation is performed in the presence of a weak magnetic field gradient ($B'_{\rm tilt} = 0.6$ G/cm) along the QMT coil axis $\hat{x}$. Note that the resulting potential $U_{\rm tilt} = \mu B'_{\rm tilt} x$ is weak relative to the crossed-optical potential ($U_0 = k_B \times 244\ \mu K$ initially), and thus does not serve as a means to change the trap depth as in other commonly used optical trap evaporation schemes [41]. Rather, the function of the tilting field is to remove the high-energy atoms which have been evaporated from the crossed-optical trap but remain in the individual optical trap beams (see Fig. 3).

We observe that the evaporation efficiency rises from $\gamma = 0.5$ in the absence of tilt, to a maximum of $\gamma = 2.3$ with a gradient of $B'_{\rm tilt} = 0.6$ G/cm. Above $B'_{\rm tilt} = 0.6$ G/cm, the gradient begins to modify the ODT potential towards the end of the ramp and we observe a decrease in evaporation efficiency. We note that the necessity of a gradient potential for ODT evaporation is peculiar to light atoms such as helium, where the influence of gravity is feeble. In heavier atoms such as ^{87}Rb, a slight tilt in the optical beams of a few degrees with respect to gravity is often sufficient to remove these atoms.

With our favorable initial conditions after the transfer in the ODT ($N = 5 \times 10^6$, $\mathcal{D} = 0.2$, and an elastic collision rate of 3×10^5 s^{-1}), we reach the transition for Bose-Einstein condensation with $N = 2 \times 10^6$ atoms at a temperature of $T = 4\ \mu$K. Figure 4 presents the measured condensate fraction as a function of temperature, normalized by the transition temperature T_c^0 of an ideal gas in a harmonic trap [42].

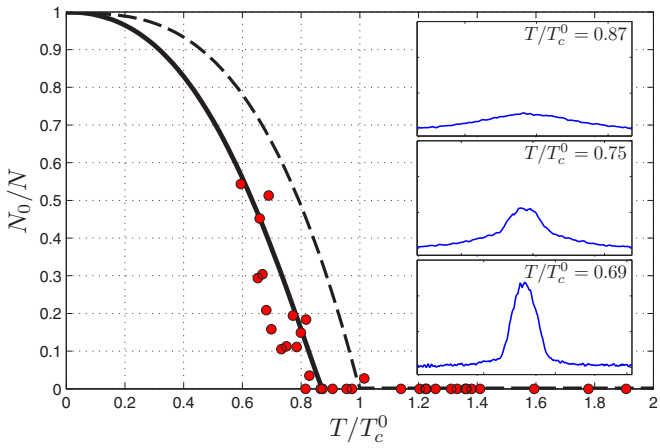

FIG. 4. (Color online) Condensate fraction across the BEC transition as a function of temperature. The single-shot experimental data (red points) are compared to the theory for an ideal Bose gas (dashed black line) and to the theory including mean-field interaction in the BEC component (solid black line) [42]. Data are plotted only for $T/T_c^0 > 0.6$ as fitting bi-modal distributions becomes unreliable at low temperatures. (Inset) One-dimensional density profiles of the gas taken after time of flight and at various temperatures across the BEC transition.

The condensate fraction and thermal gas temperature are estimated from a bi-modal fit of absorption images taken after time of flight. In the end we observe condensates of up to $N_0 = 5 \times 10^5$ atoms with no discernible thermal fraction.

In conclusion, we have demonstrated a new approach to Bose-Einstein condensation of metastable helium using a hybrid trap. The use of a magnetic quadrupole trap provides a means to reach high atomic densities allowing for efficient transfer into a crossed optical dipole trap, where fast and efficient forced evaporative cooling is performed. Several benefits result from this approach: (i) the 6-s ramp preparation time is a factor 2 shorter than the state of the art, and will facilitate rapid measurements of correlations, permitted by the ability of metastable helium atoms to be detected individually; (ii) the use of a dipole trap for the evaporation to BEC in place of the Ioffe and cloverleaf trap configurations enhances the stability of the experimental cycle; (iii) the simplicity of the coil design (two coils in anti-Helmoltz configuration) provides an excellent optical access and thus a large numerical aperture to the atoms (N.A. = 0.50). This paves the way to the investigation of multiparticle correlations in many-body Hamiltonians engineered with optical potentials. For instance, the implementation of optical lattices or optical disorder will permit the study of momentum-space correlation signals characteristic of quantum phase transitions like the Mott transition [43,44] or the Berezinskii-Kosterlitz-Thouless one in the presence of disorder [45].

We acknowledge discussions with the members of the Atom Optics group at LCF and we thank Y. Fang, T. Klafka, A. Guilbaud, F. Moron, and A. Villing for technical help. We acknowledge financial support from the Région Ile-de-France (DIM Daisy), the RTRA Triangle de la Physique, the European Research Council (Senior Grant Quantatop), the LabEx PALM (Grant No. ANR-10-LABX-0039), the International Balzan Prize Foundation (2013 Prize for Quantum Information Processing and Communication awarded to A. Aspect), the Direction Générale de l'Armement, and the Institut Francilien de Recherche sur les Atomes Froids.

[1] CMS Collaboration, J. High Energy Phys. 09 (2010) 091.

[2] L. Mandel and E. Wolf, *Optical Coherence and Quantum Optics* (Cambridge University Press, Cambridge, 1995).

[3] G. Grynberg, A. Aspect, and C. Fabre, *Introduction to Quantum Optics: From the Semiclassical Approach to Quantized Light* (Cambridge University Press, Cambridge, 2010).

[4] M. Schellekens, R. Hoppeler, A. Perrin, J. Viana Gomes, D. Boiron, A. Aspect, and C. I. Westbrook, Science **310**, 648 (2005).

[5] K. D. Nelson, X. Li, and D. S. Weiss, Nature Phys. **3**, 556 (2007).

[6] T. Gericke, P. Wurtz, D. Reitz, T. Langen, and H. Ott, Nature Phys. **4**, 949 (2008).

[7] R. Bucker, A. Perrin, S. Manz, T. Betz, C. Koller, T. Plisson, J. Rottmann, T. Schumm, and J. Schmiedmayer, New J. Phys. **11**, 103039 (2009).

[8] W. S. Bakr, J. I. Gillen, A. Peng, S. Folling, and M. Greiner, Nature (London) **462**, 74 (2009).

[9] J. F. Sherson, C. Weitenberg, M. Endres, M. Cheneau, I. Bloch, and S. Kuhr, Nature (London) **467**, 68 (2010).

[10] E. Haller, J. Hudson, A. Kelly, D. A. Cotta, B. Peaudecerf, G. D. Bruce, and S. Kuhr, arXiv:1503.02005.

[11] L. W. Cheuk, M. A. Nichols, M. Okan, T. Gersdorf, V. V. Ramasesh, W. S. Bakr, T. Lompe, and M. W. Zwierlein, Phys. Rev. Lett. **114**, 193001 (2015).

[12] W. Vassen, C. Cohen-Tannoudji, M. Leduc, D. Boiron, C. I. Westbrook, A. Truscott, K. Baldwin, G. Birkl, P. Cancio, and M. Trippenbach, Rev. Mod. Phys. **84**, 175 (2012).

[13] R. G. Dall, A. G. Manning, S. S. Hodgman, Wu RuGway, K. V. Kheruntsyanand, and A. G. Truscott, Nat. Phys. **9**, 341 (2013).

[14] R. Lopes, A. Imanaliev, M. Bonneau, J. Ruaudel, M. Cheneau, D. Boiron, and C. I. Westbrook, Phys. Rev. A **90**, 013615 (2014).

[15] R. Lopes, A. Imanaliev, A. Aspect, M. Cheneau, D. Boiron, and C. I. Westbrook, Nature (London) **520**, 66 (2015).

[16] M. D. Barrett, J. A. Sauer, and M. S. Chapman, Phys. Rev. Lett. **87**, 010404 (2001).

[17] J.-F. Clément, J.-P. Brantut, M. Robert-de-Saint-Vincent, R. A. Nyman, A. Aspect, T. Bourdel, and P. Bouyer, Phys. Rev. A **79**, 061406 (2009).

[18] Y.-J. Lin, A. R. Perry, R. L. Compton, I. B. Spielman, and J. V. Porto, Phys. Rev. A **79**, 063631 (2009).

[19] F. Bardou, O. Emile, J.-M. Courty, C. I. Westbrook, and A. Aspect, Europhys. Lett. **20**, 681 (1992).

[20] H. C. Mastwijk, J. W. Thomsen, P. van der Straten, and A. Niehaus, Phys. Rev. Lett. **80**, 5516 (1998).
[21] M. Kumakura and N. Morita, Phys. Rev. Lett. **82**, 2848 (1999).
[22] A. Browaeys, J. Poupard, A. Robert, S. Nowak, W. Rooijakkers, E. Arimondo, L. Marcassa, D. Boiron, C. I. Westbrook, and A. Aspect, Eur. Phys. J. D **8**, 199 (2000).
[23] E. Majorana, Il Nuovo Cimento **9**, 43 (1932).
[24] A. Robert, O. Sirjean, A. Browaeys, J. Poupard, S. Nowak, D. Boiron, C. I. Westbrook, and A. Aspect, Science **292**, 461 (2001).
[25] F. Pereira Dos Santos, J. Leonard, J. Wang, C. J. Barrelet, F. Perales, E. Rasel, C. S. Unnikrishnan, M. Leduc, and C. Cohen-Tannoudji, Phys. Rev. Lett. **86**, 3459 (2001).
[26] F. Pereira Dos Santos, J. Leonard, J. Wang, C. J. Barrelet, F. Perales, E. Rasel, C. S. Unnikrishnan, M. Leduc, and C. Cohen-Tannoudji, Euro. Phys. J. D **19**, 103 (2002).
[27] A. S. Tychkov, T. Jeltes, J. M. McNamara, P. J. J. Tol, N. Herschbach, W. Hogervorst, and W. Vassen, Phys. Rev. A **73**, 031603(R) (2006).
[28] R. G. Dall and A. G. Truscott, Optics Comm. **270**, 255 (2007).
[29] S. C. Doret, C. B. Connolly, W. Ketterle, and J. M. Doyle, Phys. Rev. Lett. **103**, 103005 (2009).
[30] M. Keller, M. Kotyrba, F. Leupold, M. Singh, M. Ebner, and A. Zeilinger, Phys. Rev. A **90**, 063607 (2014).
[31] R. Chang, A. L. Hoendervanger, Q. Bouton, Y. Fang, T. Klafka, K. Audo, A. Aspect, C. I. Westbrook, and D. Clément, Phys. Rev. A **90**, 063407 (2014).
[32] Fluorescence imaging with an InGaAs camera (Xeva-1.7-320 from Xenics) is used to characterize the atom cloud.
[33] J. Lawall, S. Kulin, B. Saubamea, N. Bigelow, M. Leduc, and C. Cohen-Tannoudji, Phys. Rev. Lett. **75**, 4194 (1995).
[34] G. V. Shlyapnikov, J. T. M. Walraven, U. M. Rahmanov, and M. W. Reynolds, Phys. Rev. Lett. **73**, 3247 (1994).
[35] M.-S. Heo, J.-Y. Choi, and Y.-I. Shin, Phys. Rev. A **83**, 013622 (2011).
[36] W. Petrich, M. H. Anderson, J. R. Ensher, and E. A. Cornell, Phys. Rev. Lett. **74**, 3352 (1995).
[37] R. Dubessy, K. Merloti, L. Longchambon, P.-E. Pottie, T. Liennard, A. Perrin, V. Lorent, and H. Perrin, Phys. Rev. A **85**, 013643 (2012).
[38] A. Browaeys, A. Robert, O. Sirjean, J. Poupard, S. Nowak, D. Boiron, C. I. Westbrook, and A. Aspect, Phys. Rev. A **64**, 034703 (2001).
[39] W. Ketterle and N. J. van Druten, Adv. Atom. Mol. Opt. Phys. **37**, 181 (1996).
[40] G. B. Partridge, J.-C. Jaskula, M. Bonneau, D. Boiron, and C. I. Westbrook, Phys. Rev. A **81**, 053631 (2010).
[41] C.-L. Hung, X. Zhang, N. Gemelke, and C. Chin, Phys. Rev. A **78**, 011604(R) (2008).
[42] F. Dalfovo, S. Giorgini, L. P. Pitaevskii, and S. Stringari, Rev. Mod. Phys. **71**, 463 (1999).
[43] E. Toth, A. M. Rey, and P. B. Blakie, Phys. Rev. A **78**, 013627 (2008).
[44] L. Pollet, N. V. Prokofev, and B. V. Svistunov, Phys. Rev. Lett. **104**, 245705 (2010).
[45] B. Allard, T. Plisson, M. Holzmann, G. Salomon, A. Aspect, P. Bouyer, and T. Bourdel, Phys. Rev. A **85**, 033602 (2012).